The effect of input data sampling on prestack interpolation efficacy: lessons learned from a sparsely shot and heavily structured 3D data set

Juefu Wang, Dennis Quinn, Dan Negut, Dave Ganley, Mike Perz, Muyi Kola-Ojo, and Angela Truong, Arcis Corporation, David Emery, Husky Energy Inc.*

Summary

Two different prestack interpolation methods, 5D interpolation by Fourier reconstruction and dip-scan-based data synthesis, are contrasted and compared on both synthetic data and also on a sparsely acquired and heavily structured 3D land real data set. In particular, the Fourier reconstruction algorithm's limitation in performing regular upsampling across the cmp coordinates is studied for the case of a generic upsampling problem on a well-sampled orthogonal geometry, and we attempt to gain additional insight into this upsampling limitation by computing and analyzing four-dimensional sampling operator spectra. Systematic real data testing reveals that cascading the two different interpolation methods gives good results which provide a combination of (i) regular upsampling along the crossline midpoint coordinate and (ii) gap-filling along certain shot and receiver lines which were truncated in the field because of the rugged terrain.

Introduction

Multi-dimensional interpolation by minimum-weighted-norm Fourier reconstruction was originally conceived by Liu and Sacchi (2004) and was first implemented in industry by Trad (2008). Typical algorithm usage entails interpolating across four spatial dimensions, although the algorithm is often described as a "5D interpolation" in industry circles, owing to inclusion of the temporal axis as an additional dimension (in this paper, the algorithm is referred to as "5D MWNI" for brevity). 5D MWNI has begun to enjoy routine production use and recent industry experience suggests that it can give excellent results (e.g,, Perz et al., 2009; Hunt et al., 2010; Downton et al., 2010). Despite these successes, we note that the algorithm may struggle to perform regular upsampling along the midpoint coordinates in the case of spatially aliased data (e.g., Naghizadeh and Sacchi, 2010; Wang et al., 2010). The problem is most easily understood in the frequency-wavenumber domain, where the task of regular upsampling entails annihilating aliased replicas of the spectrum of the complete (i.e., upsampled) data set. Unfortunately the annihilation process is incompatible with fundamental algorithmic action which tends to reinforce the most energetic regions of the input data spectrum, including those portions of the aliased replicas which overlap with the spectrum of the complete data. By contrast, the algorithm does a good job of infilling random gaps in coverage (i.e. instead of regular upsampling), since these gaps tend to produce random jitter, as opposed to strong and coherent patterns, in frequency-wavenumber space.

In spite of this theoretical limitation, experience shows that the use of 5D MWNI does not always lead to abject failure in CMP-domain upsampling applications in the real world. There are several possible explanations for this paradoxical observation. First, the problem can be somewhat mitigated through aspects of algorithmic craftsmanship, including judicious choice of bandlimiting constraints in the wavenumber domain (e.g., Naghizadeh and Sacchi, 2010) and/or through borrowing initial spectral weights at the current temporal frequency from a solution at a lower temporal frequency where the data are unaliased (Liu and Sacchi, 2004). Second, and probably more important, it is likely that real surveys often exhibit sufficient irregularity in sampling across at least one of the four spatial dimensions to somewhat diminish the 4D spectral replication, leading to improved results over what might be expected in the case of perfectly regular sampling. At this point it must be noted that most of the arguments and canonical examples used to illustrate the upsampling problem are based on experiments involving interpolation across one, or at most two, spatial dimensions using perfectly regularly decimated synthetic geometries. As such they fail to account for the full complexity of the sampling across the four spatial dimensions over which the interpolation proceeds in practice (the four dimensions considered in this paper are CMP-x, CMP-y, offset and azimuth). Such a reversion to lower dimensions for illustrative purposes is understandable since concepts like spectral replication due to aliasing become difficult to visualize across a four dimensional wavenumber hypercube. However, in recent work Naghizadeh and Sacchi (2010) have provided a framework for relatively simple analysis of the CMP-domain upsampling problem across all four dimensions. Specifically, they suggest computing the wavenumber response of the sampling operator which provides the mapping between the complete ideal data set and the sparsely acquired observation, as this computation helps to predict expected algorithm performance as a function of the input sampling. Although they restricted their sampling operator analysis to two spatial dimensions using synthetic acquisition templates, they point out that the concept extends straightforwardly to additional dimensions, and here we build on their work by performing a four-dimensional sampling operator analysis using a real survey geometry in an effort to gain further insight into the 5D MWNI upsampling problem.

Despite the lack of catastrophic failures in real world 5D MWNI upsampling applications, we adopt the position in this paper that the upsampling task is fundamentally incompatible with the basic algorithmic assumptions, and we are therefore motivated to seek an alternative algorithm which is better suited for regular infilling of missing CMPs. A prestack extension of the frequency-space prediction algorithm of Spitz (1991) is an obvious choice and could give good results. However, it is a "global" approach which may break down in complex structural environments where events show significant short wavelength variations such as the real data set we study in this paper. Instead, we consider another prestack interpolation algorithm which is local in nature. The algorithm (which we term "DSINTERP") is based on a dip-scan analysis of coherent energy on neighboring traces in shot and receiver gathers. It is capable of upsampling aliased data and can handle highly curved events, although it is subject to other limitations described below. Fortuitously enough, it may work well in cases where 5D MWNI breaks down and vice-versa.

This paper carries two main objectives: first, we use synthetic data and 4D sampling operator analysis to illustrate the 5D MWNI algorithmic limitations for the regular upsampling problem, as well as the DSINTERP algorithm's success in the same pursuit; second, we test the cascading of DSINTERP and 5D MWNI on a highly structured, sparse and irregular 3D land data set from the Canadian foothills, in effect leveraging the upsampling capabilities of the former algorithm together with the gap-filling capabilities of the latter.

Theory

A note on DSINTERP

DSINTERP is a coherence-guided time-space algorithm which improves the sampling of 3D volumes by inserting new shots and receivers along existing shot and receiver lines. The algorithm identifies dominant dip directions via trial dip scan across neighbouring traces, and interpolated data segments are constructed by local slant stack along these dominant directions. Unlike 5D interpolation, DSINTERP is naturally suited for upsampling along midpoint coordinates; however, because it is a local technique which uses only a small number of adjacent input traces, it cannot infill large gaps along shot/receiver lines. A second drawback is the fact that the algorithm may break down in the vicinity of intersecting dips.

4D sampling operator details

Naghizadeh and Sacchi (2010) define the sampling operator as a set of ones and zeros cast onto the output (i.e., finely sampled) multidimensional computational grid which define the positions of the existing input data. They show that in the general case of N spatial dimensions, the multidimensional input (i.e, sparsely sampled) data spectrum is given by circular N-dimensional convolution of the sampling operator spectrum with the spectrum of the complete data. They further show that the 2D sampling operator associated with perfectly regular M-fold decimation across one of the two spatial coordinates gives rise to an amplitude spectrum containing exactly M impulses embedded in an otherwise all-zero spectrum. Each sampling operator spectral impulse, including those associated with the periodic extension of the spectrum but excluding the central one (i.e., at kx=ky=0), is responsible for generating a replica of the complete data spectrum and potentially contributing to spatial aliasing. It follows that visual inspection of the sampling operator spectrum can give a preview of the possible severity of the aliasing, and therefore the expected algorithm efficacy, as a function of the input sampling configuration. For the full 4D case of upsampling one of the CMP coordinates under perfectly regular acquisition, we intuitively expect to see similar spectral impulses to the 2D case when the spectrum is viewed across the two CMP wavenumbers with offset and azimuth wavenumbers held constant.

Examples

Synthetic tests

In order to better understand algorithmic pros and cons of 5D MWNI and DSINTERP in the context of a generic CMP upsampling application, we generated a simple synthetic data set based on a regularly-sampled orthogonal real survey geometry. Shot and receiver line spacings are 390 m and 300 m, respectively, and shot and receiver spacings along lines are 180 m and 60 m, respectively, giving rise to a rectangular natural CMP bin size of 90 x 30 m. Figure 1a shows the fold on the original 90 x 30 m grid. The interpolation task entails 3:1 upsampling along the crossline axis to achieve a square 30 x 30 m final CMP grid. The underlying earth model consists of three dipping planes (dips of 10, 15, and 0 degrees from shallow to deep, all striking parallel to the crossline axis, and all producing identical reflection amplitudes) embedded in a constant velocity medium, and spatial aliasing was evident along the crossline axis on the 15 degree event prior to interpolation. Figure 1b shows the fold associated with projecting the input (i.e., uninterpolated) data onto the final 30 x 30 m output grid. In spite of the fairly regular sampling, we note that there are no purely zero fold inlines, (we would expect two out of three inlines to be missing in the case of perfectly regular sampling) and instead we observe a systematic striping pattern of alternating high and low fold; we conclude that a very mild degree of source and receiver line crookedness has given rise to sufficient midpoint scatter to ensure population of all the CMP bins. Based on our comments in the introduction, we are hopeful that this

irregular acquisition will help alleviate the upsampling limitation. Figure 2a shows a 2D slice across inline and crossline normalized wavenumbers of the incomplete data 4D sampling operator (i.e, sampling operator associated with an inline decimation factor of 3). Note that offset and azimuth wavenumbers are fixed at zero in this display. Figure 2b shows the corresponding result for the complete data (i.e., sampling operator corresponding to the data volume after upsampling). In Figure 2a we note the presence of three high amplitude impulses. The first of these is (approximately) localized in the centre of the plot at kx=ky=0 and it appears to be the primary impulse corresponding to the main spectrum of the complete data. The other two (see pink ellipses) are located along the line kx=0 at ky=+0.7 and ky=-0.7, and they presumably give rise to 4-D spectral replicas, an observation which is compatible with the intuition we gleaned from the simpler 2D analysis of Naghizadeh and Sacchi (2010). We note that these two "secondary" impulses are not present in the complete 4D sampling operator plot in Figure 2b, a finding which is again in accordance with our intuition. Figure 2c shows the 4D sampling operator spectral slices for 3-fold decimation with offset and azimuth wavenumbers fixed at midrange values, rather than at zero. Figure 2d shows the corresponding result associated with the complete data. Although it is difficult to unambiguously interpret these plots, we surmise that Figure 2c shows the superposition of three "conical" imprints associated with the three impulses displayed in Figure 2a, while Figure 2d shows a single conical imprint associated with the primary impulse. We believe that the presence of the two large spectral impulses in Figure 2a indicates the possibility of significant aliasing in the actual data spectrum--despite the lack of purely zero fold inlines--and we surmise that 5D MWNI will have trouble with the upsampling. This conjecture is confirmed in Figure 3a which shows the full offset stack of the unmigrated data after application of 5D MWNI (best-fit stacking velocities were applied to compensate for the DMO effect). The 5D MWNI result appears at first glance to be good (probably better than the result we would expect for the pure 3:1 upsampling case required for perfectly regular acquisition) , but closer inspection reveals a dimming of the middle (15 degree) reflection. The dimming is related to mis-stack associated with poor event reconstruction in the CMP gathers (not shown here), and it indicates mediocre, if not altogether poor, algorithm performance. This finding is consistent with our sampling operator analysis, and also with real world experience described in the introduction. As expected, the DSINTERP algorithm has done an excellent job of reconstructing the missing traces (see Figure 3b).

Real data experiment

The real data set under investigation is a sparsely shot 3D from the Canadian foothills. The sparse acquisition geometry suffers from two main problems: (i) the shot spacing (i.e., spacing along shot lines) is four times coarser than the receiver spacing, giving rise to a highly elongated natural CMP bin (specifically, 39 x 156 m); (ii) several shot and receiver lines have been truncated in the field because of access limitations associated with the rugged topography. In light of the relative algorithmic pros and cons discussed above, we chose to use DSINTERP to increase the shot spacing (and thereby upsample the crossline midpoint coordinate) in order to cast the data onto square bins (i.e., of size 39 x 39 m), and 5D interpolation to extend certain missing segments of source and receiver lines. Figure 4a shows a single inline from a structure stack of the original (i.e., "uninterpolated") data set cast onto the 39 x 39 m grid together with the associated surface map (inline is indicated by thick blue line in inset; shots and receivers are shown by green and red dots, respectively; note the disparity in shot and receiver spacings). The inline traverses a region of poor shot line coverage, and while it runs orthogonal to the direction of coarse CMP sampling (and thus we do not expect to see a systematic pattern of zero-fold traces), the irregular sampling has the effect that many dead and/or low fold CMPs are still apparent on the section. Figure 4b shows the corresponding image after inserting an additional 3 shot stations in between existing ones (i.e., the shot spacing has been reduced by a factor of four) using DSINTERP, thereby reducing the natural CMP bin size from 39 x 156 m to 39 x 39 m. While DSINTERP has succeeded in greatly improving image quality, it cannot infill a large chunk of missing shot line coverage (missing segment shown in black box in figure inset, and by black arrow in main pane), and low fold persists across many traces in the vicinity of the missing shot line. Figure 4c shows the result of cascading DSINTERP followed by 5D interpolation. For illustrative purposes, we parameterized the 5D interpolation algorithm in such a way that it manufactured new data along the single missing shot line segment only (thick green line in inset), and nowhere else--various alternative output data configurations and cascading strategies will be explored in the oral presentation. The additional uplift in image quality is modest but nonetheless visible (e.g. black ellipses).

Conclusions

We have studied the 5D MWNI algorithm's limitation in performing regular upsampling across the midpoint coordinates. Synthetic testing, including analysis of underlying 4D sampling operator spectra, showcases the problem and emphasizes that the underlying cause is related to the algorithm's inability to annihilate coherent 4D aliased spectral replicas. We note that our 4D sampling operator analysis constitutes a preliminary study, and further work is required to better understand the relationship between the observed spectral distribution and

5D MWNI algorithm efficacy. One test of particular interest, to be presented in the oral presentation, will involve a synthetic experiment using a Megabin acquisition template. Both 5D MWNI and DSINTERP carry relative algorithmic advantages and limitations and we have found that judicious cascading of the two algorithms has given good results on a highly structured sparse 3D land data set.

Acknowledgements

We thank Florencia Vignolo for performing the processing and Husky Energy Inc. for granting us showrights to the real data. We also thank Peter Cary for helpful discussions

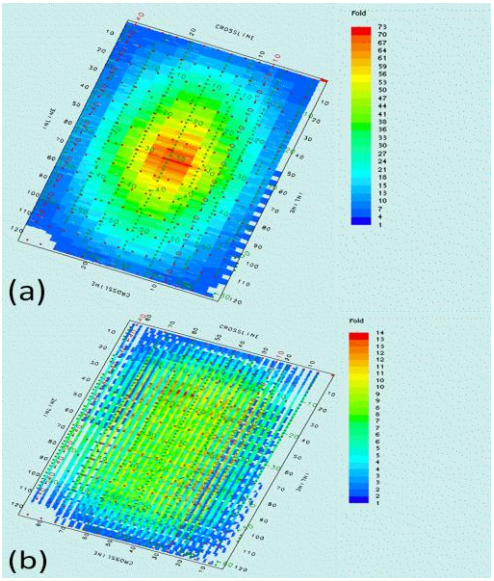

Figure 1: Fold plots based on original (i.e., uninterpolated) data for two CMP grid scenarios: (a) original 30 x 90 m grid; (b) upsampled 30 x 30 m grid.

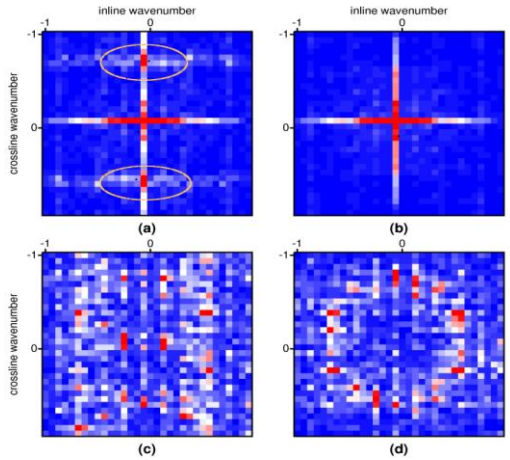

Figure 2: 4D sampling operator spectra displayed across inline and crossline wavenumbers: (a) sampling operator with decimation factor 3, offset and azimuth wavenumbers fixed at zero (b) complete data sampling operator, offset and azimuth wavenumbers fixed at zero; (c) sampling operator with decimation factor 3, offset and azimuth wavenumbers fixed at midrange (i.e., at approximately 0.5 *Nyquist); (d) complete data sampling operator, offset and azimuth fixed at midrange.

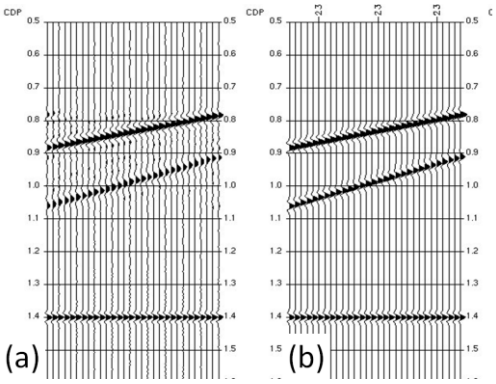

Figure 3: Full offset unmigrated stacks after upsampling to 30 x 30 m grid. (a) after 5D MWNI; (b) after DSINTERP

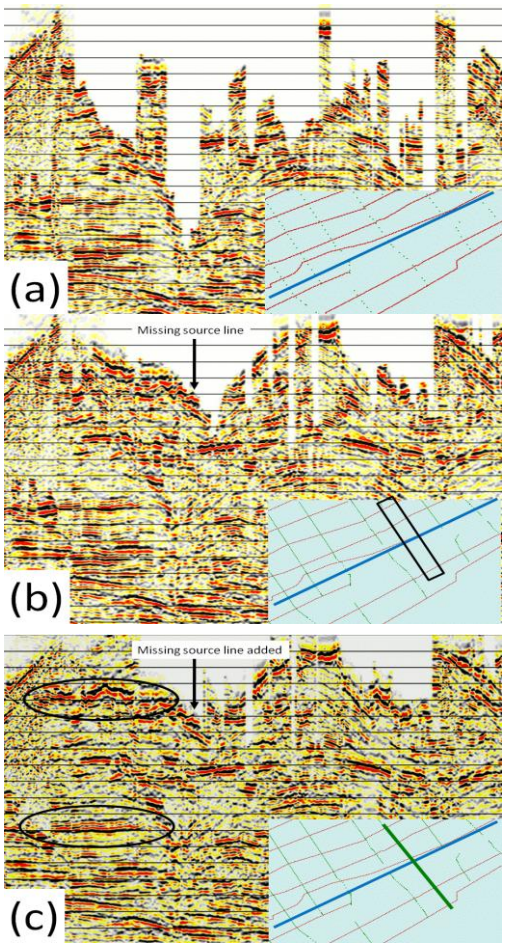

Figure 4: Real data experiments. (a) stack of raw data (main) with surface geometry shown in inset; (b) stack after DSINTERP (main) together with modified geometry map showing inclusing of new shots along existing shot lines (inset); (c) stack after DSINTERP followed by 5D MWNI. Inset shows modified surface geometry map after inclusion of new shots along existing shot lines (via DSINTERP) and inclusion of a previously missing segment of shot line (via 5D MWNI)

EDITED REFERENCES

Note: This reference list is a copy-edited version of the reference list submitted by the author. Reference lists for the 2011 SEG Technical Program Expanded Abstracts have been copy edited so that references provided with the online metadata for each paper will achieve a high degree of linking to cited sources that appear on the Web.

REFERENCES

Downton, J., D. Holy, D. Trad, L. Hunt, S. Reynolds, and S. Hadley, 2010, The effect of interpolation on azimuthal imaging and AVO: Nordegg case study: 80th Annual International Meeting SEG, Expanded Abstracts 383–387.

Hunt, L., S. Hadley, M. Hadley, J. Downton, and B. Durrani, 2008, Interpolation, PSTM, AVO, and a thin gas charged Viking shoreface in west central Alberta: CSEG National Convention, Convention Abstracts, 177–182.

Liu, B., and M. D. Sacchi, 2004, Minimum weighted norm interpolation of seismic records: Geophysics, **69**, 1560–1568, doi:10.1190/1.1836829.

Naghizadeh, M., 2010, A unified method for interpolation and de-noising of seismic records in the *f-k* domain: 80th Annual International Meeting, SEG, Expanded Abstracts, 3579–3583.

Naghizadeh, M., and M. D. Sacchi, 2010, On sampling functions and Fourier reconstruction methods: Geophysics, **75**, no. 6, WB137–WB151, doi:10.1190/1.3503577.

Perz, M., J. Wang, and Y. Zheng, 2009, Data regularization strategies for azimuth-limited prestack migration of 3D land volumes in fracture detection applications: 79th Annual International Meeting, SEG, Expanded Abstracts, 1167–1171.

Spitz, S., 1991, Seismic trace interpolation in the *F-X* domain: Geophysics, **56**, 785–794, doi:10.1190/1.1443096.

Trad, D., 2008, Five dimensional seismic data interpolation: 78th Annual International Meeting SEG, Expanded Abstracts, 978–971.

Wang, J., M. Ng, and M. Perz, 2010, Seismic data interpolation by greedy local Radon transform: Geophysics, **75**, no. 6, WB225–WB234, doi:10.1190/1.3484195.